Chinese Journal of Aeronautics, (2017), 30(2): 577–585

Chinese Society of Aeronautics and Astronautics
& Beihang University

Chinese Journal of Aeronautics

cja@buaa.edu.cn
www.sciencedirect.com

Tracking characteristics of tracer particles for PIV measurements in supersonic flows

Chen Fang [a,*], **Liu Hong** [a], **Yang Zifeng** [b], **Hu Hui** [c]

[a] *School of Aeronautics and Astronautics, Shanghai Jiao Tong University, Shanghai 200240, China*
[b] *Department of Mechanical and Materials Engineering, Wright State University, Dayton, OH 45435, USA*
[c] *Department of Aerospace Engineering, Iowa State University, Ames, IA 50011, USA*

Received 6 April 2016; revised 18 September 2016; accepted 29 September 2016
Available online 14 February 2017

KEYWORDS

Particle Image Velocimetry (PIV);
Seeding;
Supersonic flow;
Tracers;
Tracking characteristics

Abstract The tracking characteristics of tracer particles for particle image velocimetry (PIV) measurements in supersonic flows were investigated. The experimental tests were conducted at Mach number 4 in Multi-Mach Wind Tunnel (MMWT) of Shanghai Jiao Tong University. The motion of tracer particles carried by the supersonic flow across shockwaves was theoretically modelled, and then their aerodynamic characteristics with compressibility and rarefaction effects were evaluated. According to the proposed selection criterion of tracer particles, the PIV measured results clearly identified that the shockwave amplitude is in good agreement with theory and Schlieren visualizations. For the tracer particles in nanoscales, their effective aerodynamic sizes in the diagnostic zone can be faithfully estimated to characterize the tracking capability and dispersity performance based on their relaxation motion across oblique shockwaves. On the other hand, the seeding system enabled the tracer particles well-controlled and repeatable dispersity against the storage and humidity.

1. Introduction

The occurrence of shockwaves with physical interruption in compressible flows, where a significant flow deceleration occurs across a very thin region, challenges the applications of measurement techniques.[1] With the appearance of short interframing-time CCD cameras and nanosecond-duration double-pulsed Nd:YAG lasers, the recent extension of PIV technique in supersonic flows becomes mature and practical. Haertig et al.[2] performed nozzle calibration measurements in a shock tunnel at Mach number 3.5 and 4.5. Scarano[3] conducted a series of investigation on supersonic turbulent wakes as well as shockwave turbulent boundary-layer interaction. A challenging application of particle image velocimetry (PIV) was pioneered by Schrijer et al.[4,5] to investigate the flow over a double ramp configuration in a Mach number 7 flow. Schrijer and Walpot[6] pointed out that the reliability of PIV applications under extreme high-speed conditions demands smaller relaxation time of the tracer particles. Nanoparticle-based planar laser scattering (NPLS) method[7] was also

* Corresponding author.
E-mail address: fangchen@sjtu.edu.cn (F. Chen).

Peer review under responsibility of Editorial Committee of CJA.

Production and hosting by Elsevier

http://dx.doi.org/10.1016/j.cja.2016.12.033

developed to demonstrate the tracking ability of nanoparticles to capture the space-time structure in supersonic flows.

The quantitative determination of the particle tracking characteristics is commonly conducted by PIV measurements with the evaluation of the particle response time across a stationary shock wave. Earlier study demonstrated a response time of 3–4 μs for TiO_2 and more than 20 μs for Al_2O_3 particles.[8] Another PIV measurement claimed a relaxation time below 2 μs for TiO_2 particles from the particle velocity profile downstream of an oblique shockwave.[9] Then, the nanostructured Al_2O_3 aggregates around 10 nm in diameter yield a relaxation time of 0.27 μs, which is an order of magnitude reduction with respect to the compact TiO_2 nanoparticles.[10] A more recent discussion is given by Ragni et al.[11], who obtained the relaxation time of different solid particles in the range of 0.4–3.7 μs based on a systematic investigation. However, few investigation takes the characterization of compressibility and rarefaction effects into consideration. This motivates the present efforts to experimentally and theoretically analyze the particles' motion allowing for measurement conditions variation to develop the seeding-particle-selection and seeding-distribution techniques within a higher Mach number regimes.

The experiments were conducted by PIV techniques in Multi-Mach Wind Tunnel (MMWT) of Shanghai Jiao Tong University (SJTU). The tracer particles' motion across a shockwave was theoretically modelled considering compressibility and rarefaction effects and then experimentally analyzed from PIV measurements. It can yield qualitative information on particles' motion to estimate the available size of tracer particles in selection before experiments and analyze their effective aerodynamic diameters after experiments. In order to reach the requirements for tracer particles, advances in the seeding system integrating a pressurized vessel with a fluidized bed enabled the seeded particles to track the supersonic flows.

2. Experimental apparatus and procedure

Fig. 1 shows the diagram and components of MMWT, which is capable of providing supersonic and hypersonic flows with nominal Mach number Ma_∞ = 2.5, 3, 4, 5, 6, and 7, respectively. The blowdown-suction operation pattern extends the test duration time up to 20 s. The present experiments to analyze the characteristics of particles are operated at the free-stream condition of nominal Mach number 4. The velocity of the supersonic mainflow in the test cabin is 800 m/s with total pressure of 0.5 MPa and total temperature of 400 K.

2.1. PIV system setup

Fig. 1 shows a double-frame digital PIV system composed of the laser, CCD camera, and synchronizer. The solid-state frequency-doubled Nd:YAG laser with a wavelength of 532 nm has a nominal energy of 500 mJ (stability ±4%) per pulse. Lasers are available with pulse width about 5 ns, and repetition rate of 1–10 Hz. The test cabin holds three windows with 200 mm diameter, which can be optically accessible for PIV measurements. PIV pictures within the illuminated region are taken from the front view by an IPX-11M CCD camera (4000 × 2672 pixels, 11 M resolutions, 12 bits). The camera uses high-performance progressive-scan interline CCD chips, capable of acquiring two images with a minimum pulse separation of 200 ns and framing rate of 5 Hz. The time interval between pulses is a critical parameter, i.e. the particles moving time t, for matching the PIV system to the flow velocity. The particle images are recorded at 5 Hz resulting in 50 image pairs per tunnel run. A 105 mm SIGMA lens at $f\# = 2.8$ is carefully chosen to gain the particle images with sufficient collected energy and reduce the image blur due to aero-optical aberrations. The camera is fitted with a narrowband-pass 532 nm filter to minimize ambient light interference and almost tangential to the wall to alleviate the reflections.

2.2. Particles' seeding technique

Fine and non-agglomerated particles are required for PIV measurements under the extreme high-speed conditions. TiO_2 particles with nominal diameter of 30 nm are chosen as the tracers in the present flow measurement. However, the humidity and prolonged storage make these particles a strong tendency to form agglomerates several times larger than the

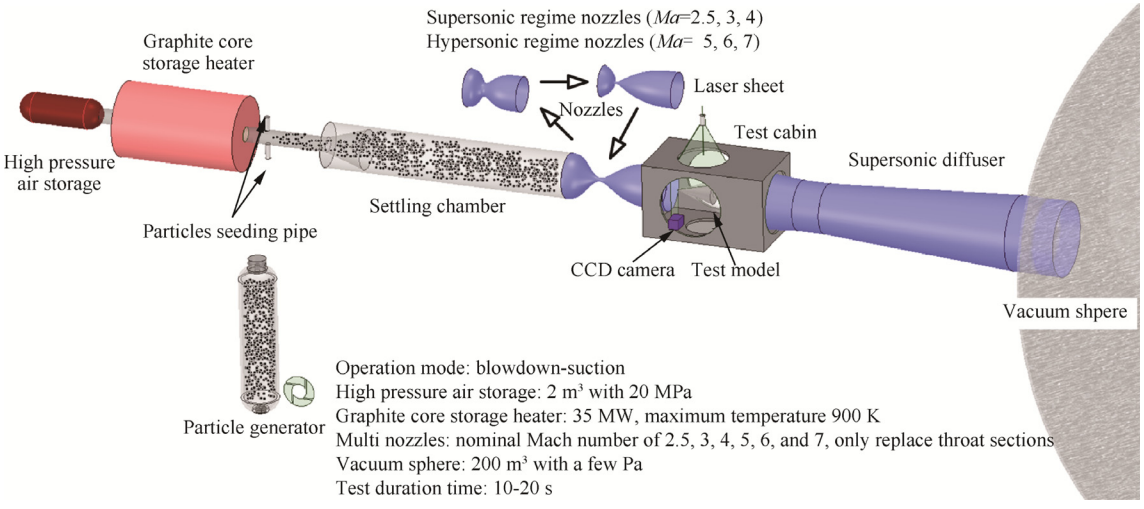

Fig. 1 Multi-Mach numbers wind tunnel (Ma_∞ = 2.5–7) and PIV system setup.

primary sizes. A tracer particles' seeding system is newly designed to disperse the particles (Fig. 2). The interactive force among the particles resulted from the charge of solid tracer particles will be negligible next to nothing in consideration of the electric conductivity of the metallic particle seeding device. In contrast, a mechanism is developed to disperse the dehydrated powders in a fluidized-bed like device in a once-molded vessel with high tensile and compressive strength of 16 MPa, which is driven by a swirling dry air jet with both high pressure gradient and high momentum. It is expected to ensure particles fully mixing with the flow and to make the aerosol (the mixture of air flow and suspended particles) uniformity in the PIV measured region. This device also vastly simplifies the process to supply and clean the particles during the experiments. The jet flow with 2 MPa beyond the mainflow will provide a suitable flow rate of 0.01 kg/s carrying the seeding particles, yielding appropriate concentration among several preliminary runs.

3. Characteristic analysis of tracer particles

3.1. Tracers' motion across a shockwave

In an ideal situation, the primary particles hardly shield each other in collisions with gas molecules if the mean free path of the molecules is much larger than the particles' size. The monodisperse solid particles of small size can conventionally be treated as spheres with an aerodynamically equivalent diameter. According to the general theory of solid tracer particles motion in gas flows described by Melling[12], only the viscous and inertia terms are always considered in Basset-Bousinesq-Oseen equation. Therefore, the particle velocity U_p typically responses to a stepwise variation in surrounding flow velocity U with an exponential decay law:

$$U_p(t) = U\left[1 - \exp\left(-\frac{t}{\tau}\right)\right] \tag{1}$$

where t is the tracer particles' moving time and τ the relaxation time to qualify the particle's response. It is characterized in terms of the drag coefficient C_D as

$$\tau = \frac{4}{3} \times \frac{\rho_p d_p^2}{\mu} C_D^{-1} Re_p^{-1} \tag{2}$$

The particle Reynolds number Re_p is dictated with respect to the relative velocity between the particle velocity and the gas velocity far from the particle surface as:

$$Re_p = \frac{\rho_p |U_p - U| d_p}{\mu} \tag{3}$$

where μ is dynamic viscosity of the flow, and ρ_p and d_p are the density and diameter of the particle, respectively.

The experimentally inferred particle relaxation time τ becomes a crucial factor for the velocity measurement in high-speed flows. When a particle with initial velocity $U_p(0)$ is seeded into the flow, the particle will accelerate with the surrounding flow at the rate of $1/\tau$. The corresponding velocity $U_p(t)$ gradually increases close to, but never up to the flow velocity U. Similarly, the tracer particles across a shockwave, as shown in Fig. 3, decelerate with an exponential decay to follow the actual flow streamlines downstream of the shockwave in a finite time instead of a theoretical discontinuity at the shockwave. Here, a dimensionless velocity U^*, i.e., the slip velocity of a particle is defined as

$$U^* = (U_{pn}(t) - U_{n2})/(U_{n1} - U_{n2}) = e^{-\frac{t}{\tau}} \tag{4}$$

where e is natural logarithm, $U_{pn}(t)$ is specified as the normal velocity of the particle, U_{n1} and U_{n2} represent the normal velocity of the flow before and after the shockwave. It is assumed that all seeded particles would be well-mixed and uniform while they travel till the vicinity of the shockwave.

Further information regarding the response of particles across shockwaves can be found in Dring[13] or Tedeschi et al.[14] Such a procedure was adopted in the previous investigations[2,15,16] to obtain the velocity profile across a planar oblique

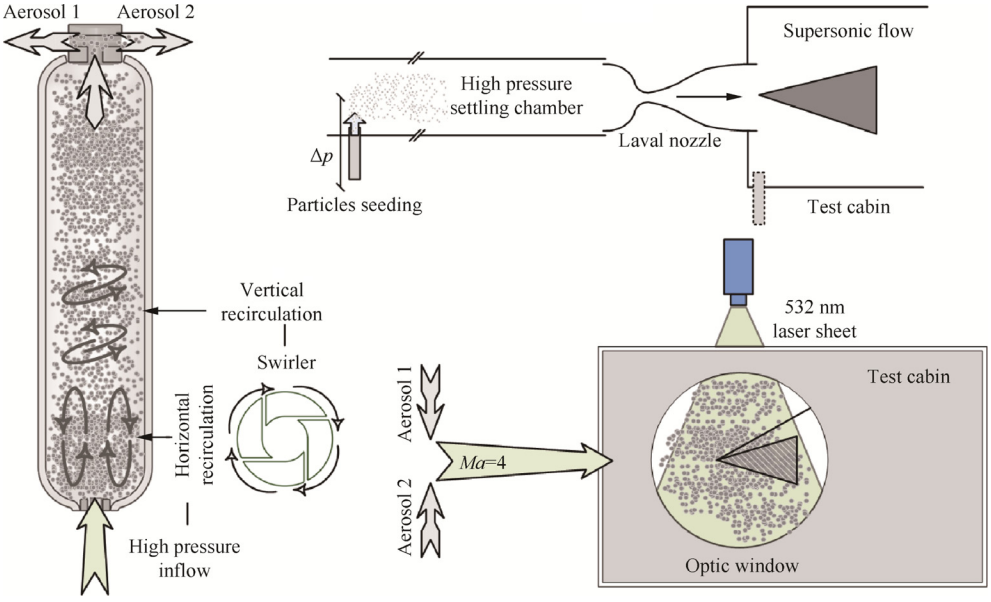

Fig. 2 Tracer particles' seeding system.

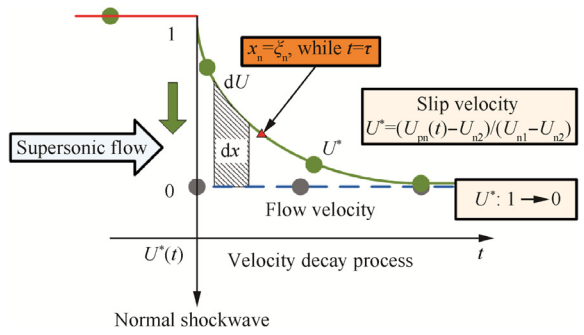

Fig. 3 Motion of tracer particles across a shockwave in supersonic flows.

shockwave, following the fact that the tracer particles decelerate gradually due to inertia.[9] In those supersonic flow tests are conducted over the wedge with a small deflection angle,[5,10,11] the induced shockwave strength i.e. normal Mach number is typically lower than 1.4. By treating the particle's deceleration across a shock in a piecewise way, the relaxation is always given to be approximately linear[11] as follows:

$$\frac{x_n}{\xi_n} \approx \frac{t}{\tau} = -\ln U^* \tag{5}$$

where x_n is the location normal to the shockwave, and ξ_n the relaxation distance of a particle normal to the shockwave. Although Eq. (5) conveniently quantifies the particle's time response of τ, it would become invalid in case that shockwave is obviously stronger than the precondition. With the inspiration of Ragni et al.[11], an analytic model with a wide range of adaptability has been proposed in the previous work[16] to estimate the relaxation process of tracer particles. By further integrating over the time range of [0, t], the dimensionless displacement $x^* = x_n/\xi_n$, can be derived as an explicit function of dimensionless particle slip velocity U^*:

$$x^* = e(U^* - \ln U^* - 1) \tag{6}$$

where the particle relaxation distance

$$\xi_n = \tau[U_{n1} - (U_{n1} - U_{n2})/e] \tag{7}$$

Obviously, the dimensionless displacement x^* always obeys the relationship with the dimensionless slip velocity U^* in Eq. (6), which is determined by the ratio of t/τ. In general, the present model of Eq. (6), which properly represents the particles relaxation process regardless of the effects of shockwave strength, has outperformed the empirical expression of Eq. (5).

By using the normal shockwave relations, Eq. (7) can be clearly changed into

$$\frac{\xi_n}{U_{n1}\tau} = \frac{e(\gamma+1)Ma_{n1}^2 - 2Ma_{n1}^2 + 1}{e(\gamma+1)Ma_{n1}^2} \tag{8}$$

It can be seen that normal Mach number Ma_{n1} affects to a tiny extent in view of the fact that the right term in Eq. (8) only varies from 0.69 to 0.84 for supersonic flows, where the ratio of specific heat γ is equal to 1.4. For a given particle relaxation distance ξ_n, the relaxation time of tracer particle τ is therefore approximately reciprocal to the flow velocity before the shockwave U_{n1}. That means increasing U_{n1} and/or reducing ξ_n yields less requirement of the relaxation time τ. Clearly, smaller τ for particles applied in PIV measurements would be preferable, which plays an important role in the relaxation process.

3.2. Particles selection criteria

By revealing the effects of time ratio t/τ, i.e., slip velocity U^* of the particles on the dimensionless displacement x^*, a semi-elasticity concept,[17] also as a popular economic tool, is introduced to analyze the responsiveness of a function to changes in parameters. Algebraically, the semi-elasticity S of a function f at point x is

$$Sf(x) = \frac{f'(x)}{f(x)} = \frac{d\ln f(x)}{dx} = \frac{d\lg f(x)}{dx} \tag{9}$$

Generally, semi-elasticity indicates variables sensitive to a percentage change, which is useful to evaluate how the change in slip velocity U^* affects the particle dimensionless displacement x^*. From this point of view, the semi-elasticity of dimensionless displacement x^* is dominated by the variable slip velocity U^* as the following equation:

$$S(x^*) = (1 - U^*)/[U^*(U^* - \ln U^* - 1)] \tag{10}$$

It can be seen in Fig. 4 that a percentage change in x^* is divided by a dimensionless change in U^* relative to the initial slip velocity $U^* = 1$ ($t = 0$). As illustrated in Fig. 4, the ratio of t/τ is also crucial (Point A) while $S_{min} = e(e-1)$ at $U^* = e^{-1}$. Consequently, the particle relative velocity $|U_p - U|$ downstream of a shockwave is conveniently quantified while $t/\tau = 1$, i.e., $U^* = e^{-1}$. The percentage changes in displacement x^* become convergent while closing to S_{min} and vice versa. Interestingly, the present model also easily finds the recommended parameter t/τ, which affects the particle deviation movement at an acceptable finite extent. When the ratio of t/τ varies from 0.25 (Point C) to 3 (Point B), not much changes of x^* (no more than 10%) is in response to changes of U^*. This credible range of 0.25–3 would be acceptable for tracking the discontinuities of the shockwave in the relaxation process.

If the particle Reynolds number Re_p is small ($Re_p \ll 1$), the drag coefficient C_D can be given by Stokes' drag law[18] as

$$C_D = 24/Re_p \tag{11}$$

It should be noted that this linear dependence of drag on the relative velocity is only available to the incompressible and continuum flow, but it represents a conservative estimate of the tracking ability of particles for small relative velocity. Eq. (9) can be therefore greatly simplified:

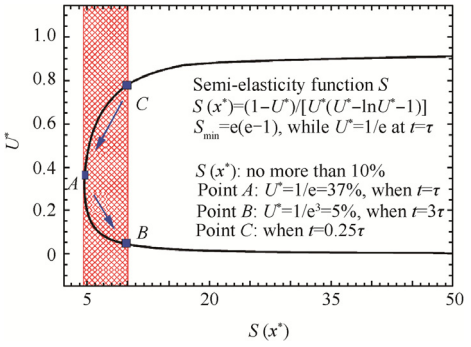

Fig. 4 Semi-elasticity of relaxation process for responsiveness of slip velocity.

$$\tau = \frac{\rho_p d_p^2}{18\mu} \tag{12}$$

where $\mu = 6.4 \times 10^{-6}$ N·s/m^2, which is obtained from Sutherland equation at the present measurement conditions with static pressure (3.1 kPa) and static temperature (96.4 K). Eq. (12) is convenient to calculate the relaxation time of tracer particles, which directly depends on the particles' diameter.

3.3. Compressbility and rarefaction effects

In order to gain a further insight into the particle dynamics in supersonic regimes, which generally exceeds Stokes' drag regime ($Re_p \ll 1$), some governing dimensionless parameters are introduced to consider the compressibility and rarefaction effects. For the sphere correction data at a higher relative Reynolds number Re_p, a large number of empirical expressions have been proposed to describe the drag coefficient C_D. When the relative particle velocity is comparable to the gas speed of sound, the compressibility should be considered, which is characterized by the relative Mach number Ma_p as

$$Ma_p = \frac{|U_p - U|}{\sqrt{\gamma RT}} \tag{13}$$

where γ is specific heat ratio of gas flow and R is gas constant. In other words, weaker relative Mach number shows better tracking performance. Considering the low density of gas flow, which usually appears under supersonic simulation conditions, the particle Knudsen number Kn_p is no longer small. It is defined as the ratio of the mean free path of the surrounding molecules to the particle diameter, which can be written in terms of the particle Mach number and Reynolds number as

$$Kn_p = \frac{l}{d_p} = \sqrt{\frac{\pi\gamma}{2}}\left(\frac{Ma_p}{Re}\right) \tag{14}$$

If the flow hardly satisfies $Re_p \ll 1$, it will lead to a deviation between the mean molecular velocity and the mean particle surface velocity since the molecules near the surface lack sufficiently high collision rate. In that case, the drag coefficient is no longer linearly dependent on the relative velocity.

As listed in Table 1,[9–11,14,16,19–21] several representative PIV measurements with shockwave structures are summarized. Generally, the dimensionless parameters Re_p, Kn_p, and Ma_p, which determine the drag coefficient, are all typically not small enough to neglect their effects for PIV measurements in supersonic flows. In view of those flow regimes characterized by Re_p, Kn_p, and Ma_p, the flow around the particles can be considered as laminar, transition, and compressible flow. Loth[22] developed a prediction model of the drag coefficient, which is supported by experimental and numerical results, to describe the flow physics around a particle. In the ranges of the dimensionless parameters from Table 1, the drag coefficient is dominated by rarefaction effects for $Re_p < 45$. The drag decreases resulted from the slip effects as the Knudsen number increases. When the particles are assumed in thermal equilibrium, the empirical expression of the drag coefficient in the rarefaction-dominated regime is defined as

$$C_D = [24/(Re_p f_{Re_p} f_{Kn_p} f_{Ma_p})]/(1 + Ma_p^4) \tag{15}$$

$$f_{Re_p} = 1 + 0.15 Re_p^{0.687} \tag{16}$$

$$f_{Kn_p} = 1/\{1 + Kn_p[2.514 + 0.8\exp(-0.55/Kn_p)]\} \tag{17}$$

$$f_{Ma_p} = \frac{\frac{(1+2s^2)\exp(-s^2)}{s^3}\Big/\sqrt{\pi} + \frac{(4s^4+4s^2-1)\mathrm{erf}(s)}{2s^4} + 2\sqrt{\pi}/3s}{1 + \left\{\left[\frac{(1+2s^2)\exp(-s^2)}{s^3}\Big/\sqrt{\pi} + \frac{(4s^4+4s^2-1)\mathrm{erf}(s)}{2s^4}\right]\Big/1.63 - 1\right\}\sqrt{Re_p/45}} \tag{18}$$

where $s \equiv Ma_p\sqrt{\gamma/2} = Kn_p Re_p/\sqrt{\pi}$.

This expression with correction factors of Eq. (15) has been proven quite robust in comparison with experimental and DSMC data. Fig. 5 illustrates the compressibility and rarefaction effects on the drag coefficient within the concerned range of governing parameters from Table 1. Also shown in Fig. 5 is the probable parameter ranges for present PIV measurements. For these conditions in the present study, the drag coefficient is dominated by the variation of particle Knudsen number Kn_p. Besides, the effect of particle Mach number Ma_p is small but not negligible. Since the magnitude of the relaxation time is primarily dependent on the particle size, this accurate estimate of the particles relaxation is also constrained by appropriate particle tracking. It can be clearly seen that the actual drag coefficient tends to be smaller than Stokes' resistance so that Eq. (11) would conservatively estimate the desired size of the tracer particles for tracking the flow across a shockwave. According to Eqs. (2) and (15) and the probable parameters of the present study, the corresponding diameter of tracer particles is preliminarily calculated as only approximately the one-fifth of the overrated value from Eq. (11) for the same relaxation time τ.

Table 1 Flow regimes for PIV measurements in supersonic flows.

Item	Re_p		Kn_p	$Ma_p = Kn_p \cdot Re_p \cdot \sqrt{2/\pi\gamma}$
Parameter range	$0.01 \leqslant Re_p \leqslant 10$		$0.1 \leqslant Kn_p \leqslant 10$	$0.4 \leqslant Ma_p$
Flow physics	Laminar flow		Transition flow	Compressible flow
References	Re_p	Kn_p	Ma_p	PIV specification
Scarano et al.[9]	1.8	0.3	0.4	Compressible wake, free stream: Ma = 2, U = 504 m/s, TiO_2: 500 nm
Tedeschi et al.[14]	0.5	1	0.2	Oblique shockwave, free stream: Ma = 2.3, U = 550 m/s, latex: 500 nm
Chen et al.[16]	0.4/0.3	1.5/2	0.4/0.5	Oblique shock, free stream: Ma = 4/7, U = 800/1200 m/s, TiO_2: 300 nm
Koike et al.[19]	4	0.15	0.4	Trans-injection, free stream: Ma = 1.8, U = 460 m/s, dioctyl sebacate: 1 μm
Humble et al.[20]	0.7	0.5	0.2	Oblique shockwave, free stream: Ma = 2, U = 504 m/s, TiO_2/Al_2O_3: 500 nm
Ghaemi et al.[10]				
Ragni et al.[11]				
Mathijssen et al.[21]	0.4	0.3	0.1	Delta wing, free stream: $Ma \approx 2$, U = 500 m/s, Aerosol: 700 nm

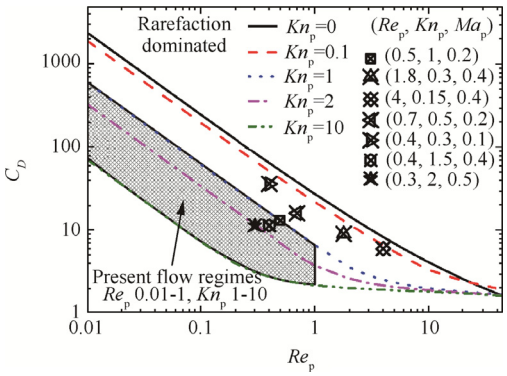

Fig. 5 Rarefaction and compression effects on drag coefficient of a particle in thermal equilibrium, expressed in Eqs. (15)–(18) by Loth[22] for $Re_p < 45$.

The time interval t is presumed at 500 ns for the measured flowfield (nominal Mach number 4, freestream velocity 800 m/s) in the present PIV set-up along with the field of view 180 mm × 180 mm, camera resolution 4000 × 2672 pixels, interrogation area 32 × 16 pixels. A further analysis will be discussed about the relaxation process via the particles of various sizes. As depicted in Fig. 6, when the air flow through a 15° wedge at freestream Mach number 4, an oblique shockwave with normal Mach number Ma_{n1} of 1.84 is induced on the edge with an angle of about 27°. The curves show the component of the particle velocity normal to the shock as a function of the normal distance downstream of the shock.

Clearly, smaller particles, which decelerate rapidly downstream the shock, would be preferable as PIV tracers in the high speed flow. Considering the desired ratio of t/τ = 0.25–3, the obtained diameter of the typical TiO_2 particles (the particle density ρ_p is generally 4.23 × 10^3 kg/m^3) is rounded to the nearest 10 as 20–50 nm after taking into account the compressibility and rarefaction effects. It will be preferable to ensure good tracking of supersonic flow within a fixed time interval t = 500 ns. It is also seen that the particles no more than 50 nm recover rapidly across an oblique shockwave while decelerating close to the gas velocity downstream of the shock only in a short distance of about 0.5 mm. In other words, the tracer particles in nanoscales are in need for successful PIV applications in supersonic regime. The seeding technique of

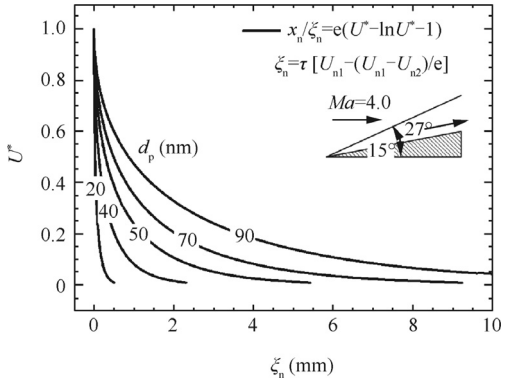

Fig. 6 Relaxation process across an oblique shockwave in Mach number 4.0 flow.

tracer particles would face a challenge to satisfy this strict condition. The corresponding experiments are then conducted to validate the feasibility of the previous characteristic analysis on the tracking performance of PIV tracer particles over an induced shock wave in supersonic flows.

4. Results and discussions

The calibration tests have been firstly performed in the empty wind tunnel operation at freestream Mach number 4. A pair of images is analyzed with cross-correlation algorithm using Micro Vec2 software employing 32 × 16 pixels with 50% overlapping. The resulting time-averaged velocity vector distributions of tracer particles are also compared to calculated values from total pressure rake. A rather homogeneous velocity field in spatial distribution is demonstrated in the core flow. The averaged PIV measured velocity field for free stream is very close to the calculated velocity with the uncertainty of less than 2%.[16] TiO_2 particles with a nominal crystal size of 30 nm showing better dispersity are finally used.

The present work assumes ideal imaging and tracking conditions, i.e., pixelization effects are neglected. The time interval t between exposures is set as 500 ns, which is assumed small enough to neglect the time averaging effect on the velocity. Furthermore, the averaging effect of the finite interrogation window size is neglected as well. The velocity considered is that of the particle, which may differ from the actual local flow velocity due to particle relaxation. The magnitude of the velocity error is reduced in the measurement by amplitude modulation in the cross-correlation. The velocity vector field is calculated from 200 image pairs in several repetition runs to minimize the position and velocity error due to any shock movement or displacement of the field of view.

The flow over 2D sharp wedges of 35 mm in length and 20 mm in width with 15° and 30° in deflection angle θ are measured by PIV system with TiO_2 tracer particles of nominal crystal size 30 nm. The models made by stainless steel are mounted downstream of the nozzle exit in the test cabin. Acquired velocity distribution of the external flow field is given to compare with Schlieren photos and diagnose the flow phenomena. Only the shockwave located at the model leading edge, which appears as steady compressible flow, is considered for the present experimental investigation. The light sheet covers part of the freestream and the induced shock near the model.

As shown in Fig. 7, PIV data are very much in accordance with Schlieren visualization and theoretical data derived from oblique shock relations. The results are also summarized in Table 2. In the present experiments, the shockwave always attaches the tip of the wedge models. Theoretically, when Mach number 4 flow deflects more than 38°, a detached bow shockwave will come into being. It is still noted that when the flow deflection angle is 30° for the 60° wedge model, the leading edge shockwave shows in a curve shape. In this case, the induced oblique shockwave strength Ma_{n1} is nearly up to 3.0 and the relative particle Mach number Ma_p is considered as 0.77 at U^* = 1/e. Therefore, the particles motion downstream the strong shockwave shows an undesired tracking performance so that the measured particle velocity at most recovers to 164.8 m/s with approximated 8% deviation to theoretical value. Further differences may be ascribed to the shot-

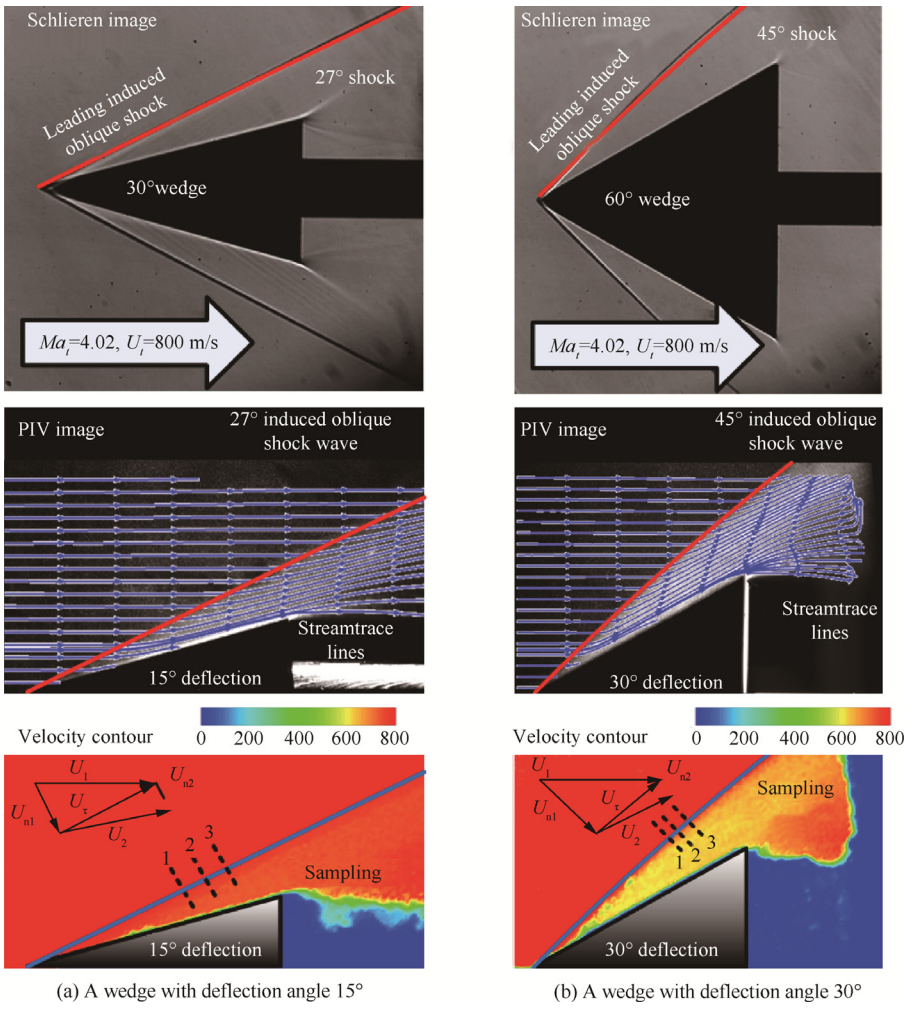

(a) A wedge with deflection angle 15° (b) A wedge with deflection angle 30°

Fig. 7 PIV images and measured flow field over 2D wedge models vs Schlieren images.

to-shot jitter of the shock position and optical aberration effects across shock waves.

By sampling and averaging U_p normal to the theoretical shock at several locations from PIV data as shown in Fig. 7, the slip velocity U^*, which is nondimensionlized by the theoretical solution of the fluid velocity U_{n1} and U_{n2}, can be calculated and illustrated in Fig. 8(a). As expected, the steep velocity gradient across the shockwave causes the tracer particles to decelerate slower than the fluid and gradually approach the downstream velocity, although the velocity profiles for both models unfortunately fluctuate in the slowly recovery segment due to the probable interaction with the wake of the wedge. The results experimentally confirm that the particle velocity after a weaker shockwave, which is induced by 15° wedge model, recovers more rapidly to the gas velocity in a shorter relaxation distance. On the contrary, a worse particle tracking appears for the stronger shockwave (30° wedge model) because the particle velocity still has a deviation to the gas velocity even in a much longer distance.

However, the relaxation distance ξ_n is hardly identified on account of the unclear shockwave location. In order to fit the particles velocity decay, a further analysis on the curve line

Table 2 Induced shockwave characteristics over wedge models.

Parameter	15° wedge			30° wedge		
	PIV	Schlieren	Theoretical	PIV	Schlieren	Theoretical
Shockwave angle β (°)	27.2	27.2	27.0	45.2	45.4	45.1
Freestream velocity U (m/s)	808.2		797.8	810.3		797.8
Velocity U_{n1} (m/s)	369.4		362.2	575.0		565.1
Shockwave strength Ma_{n1}	1.88		1.84	2.92		2.87
Velocity U_{n2} (m/s)	155.2 (recovery)		151.1	164.8 (recovery)		151.9
Relative Mach number Ma_p	0.39 at $U^* = 1/e$ while $t = \tau$			0.77 at $U^* = 1/e$ while $t = \tau$		

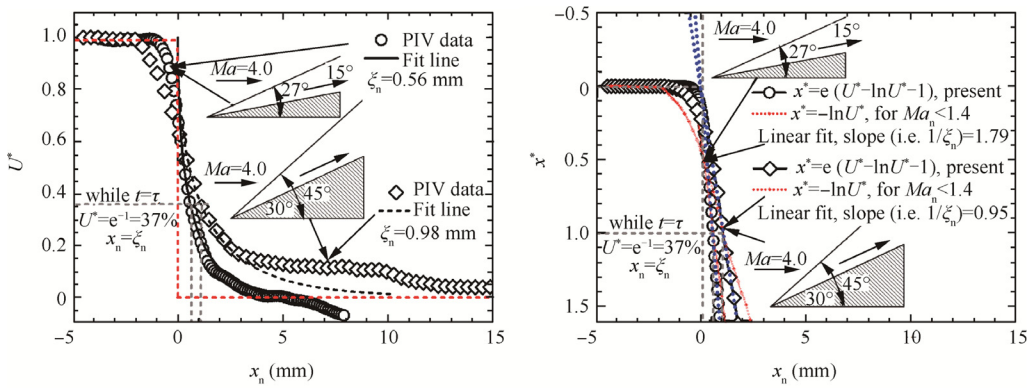

Fig. 8 PIV measurement of normal velocity across shockwave.

x^* versus x_n is illustrated in Fig. 8(b). A clearly linear relation as the definition demonstrates Eq. (6) well matches the particle motion quite better than Eq. (5). Herein, the reference zero point of x_n coordinate axis is easily identified as the point where this linear fitting line (blue dot lines in Fig. 8(b)) intersects the line $x^* = 0$. Therefore, the relaxation distance ξ_n is the reciprocal of the linear fitting slope (1.79 for 15° wedge and 0.95 for 30° wedge), i.e., 0.56 mm for 15° wedge and 1.05 mm for 30° wedge. It is also observed as the value of x_n while $x^* = 1$, i.e., $U^* = 1/e = 37\%$ at $t = \tau$. The particle motion described by Eq. (5) is only satisfied at this point, and the apparently nonlinear relation will give a higher relaxation distance ξ_n so as to overestimate the values for both wedge models with oblique shock strength $Ma_{n1} > 1.4$. Therefore, further taking into account the characteristic of the supersonic flow makes the present model of Eq. (6) to exactly capture the particle tracking process. With the estimated relaxation distance ξ_n, the corresponding fit line plotted in Fig. 8(a) demonstrates a good agreement with the velocity decay as well.

Since the storage and humidity tends to cluster the seeding particles as porous agglomerates, these particles are found to be approximately 200 nm inspected by a scanning electron microscope (SEM) imaging. SEM can only be used to the geometric features of the compact agglomerates in the seeding system before dispersing into the main flow. However, owing to the inevitable agglomeration in the seeding process, the actual aerodynamic diameter of the tracking particles accessible to the test section, which determine the relaxation process across a shockwave, is still unknown. It is noteworthy that the combination of Eqs. (2), (6), (7) and (15)–(18) can qualify the effective aerodynamic diameter of the tracer particles based on the collected velocity distributions. The particle relaxation time τ across the incident shockwave can be easily analyzed according to Eq. (7). The relaxation time is mainly dependent on the size of primary particles, although there may be a distribution of particle with variable sizes. Note that the no-shielding assumption exists while the primary particles size is much smaller than the mean free path of the gas molecules. Moreover, the particles in nanoscales present much more stable illumination. As a matter of fact, the applied particles for two wedge models may be considered as the similar size due to the same kind of particles, seeding system and wind tunnel. In practice, the relation between the relaxation time and the corresponding size renders us a possibility for investigating the particles size from PIV measurements across the shockwave.

The particles tracking performance and seeding efficiency are therefore evaluated. By performing an iteration based on Eqs. (2), (6) and (7) integrated with Eqs. (15)–(18), which is robustly fit to the rarefaction dominated regime as discussed before, the particle size can be obtained. It is noted that this value is unable to attain directly in that the particle relative parameters, Re_p, Kn_p are highly dependent on the unknown particle diameter. Attributable to the compressibility and rarefaction effects, the actual particle size in the experiments for both models is evaluated to be almost the same, 40 nm for 15° wedge and 50 nm for 30° wedge, respectively. In comparison with the other calculations, all the estimated results of the particle size rounded to the nearest 10 and the corresponding flow parameters are listed in Table 3. It can be seen in Fig. 9 that a significant difference in the particle sizes for the

Table 3 Relaxation time and diameter analysis of tracer particles.

Parameter	15° wedge		30° wedge	
	Eq. (6)	Eq. (5)	Eq. (6)	Eq. (5)
Relaxation distance (mm)	0.56	0.98	1.05	2.11
Relaxation time (μs)	1.97	3.44	2.54	5.11
Eq. (11) particle diameter (nm)	230	310	260	370
Eq. (15) corrected particle diameter (nm)	40	70	50	100
SEM particle diameter (nm)	200			
Nominal particle diameter (nm)	30			
Relative Reynold number	0.05	0.09	0.13	0.26
Particle Knudsen number	11.48	6.60	8.95	4.44
Relative Mach number	0.39	0.39	0.77	0.77

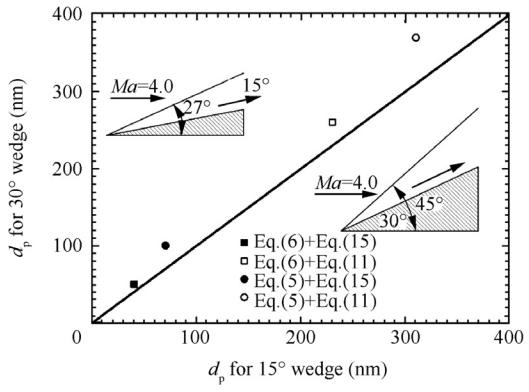

Fig. 9 Aerodynamic diameters of seeding particles.

two wedges, which is calculated from empirical Eq. (5), also gives a clear disproof for its limited reliability. On the other hand, Eq. (11) approximately five times overrates the particle size as the actual drag coefficient tends to be lower than Stokes' drag law so that it is also proven unreasonable.

Interestingly, the estimated size of the tracer particles is found to be very close to their nominal diameter, even though the limitation of the PIV spatial resolution is considered. This value is greatly smaller than SEM inspection data, which only respects the storage status as a result of inevitable humidity and carriage. Therefore, the seeding system demonstrates a great capability to mitigate the agglomeration of tracer particles. On the other hand, TiO_2 particles with nominal 30 nm diameter are proven as the candidate with better tracking characteristics with negligible agglomeration. In general, the tracking deviation of particles may slightly influence the measurement of the shock thickness, whereas the particles can capture the actual flow field over a wedge with a relatively accurate velocity before and after the shockwave.

5. Conclusions

(1) An extension of particles response model is proposed for supersonic research compared to the traditional model limited to $Ma_n < 1.4$ regime. The criterion of selecting appropriate particles is described to satisfy the relationship of the relaxation time: $t/\tau = 0.25–3.00$. The desired particles to ensure effective capturing of the flow field under well-controlled conditions of Mach number 4 should be approximately 20–50 nm in diameter with the time interval $t = 500$ ns in consideration of compressibility and rarefaction effects.

(2) Powders of TiO_2 particles with 30 nm diameter are used in the present work for PIV measurements. The advances in the seeding system by integrating a pressurized cyclone with a fluidized bed demonstrate a distinct improvement of seeding performance. These tracers in nanoscales for PIV measurements prove successful to capture the actual flow field over a wedge with a relatively accurate velocity before and after the shockwave. That the actual size of tracer particles is estimated to be very close to their nominal diameter shows a high dispersity efficiency of the seeding system.

Acknowledgements

This study was supported by the National Natural Science Foundation of China (Nos. 11672183, 91641129 and 91441205).

References

1. Scarano F. Overview of PIV in supersonic flows. *Top Appl Phys* 2008;**112**(1):445–63.
2. Haertig J, Havermann M, Rey C, George A. Particle image velocimetry in Mach 3.5 and 4.5 shock-tunnel flows. *AIAA J* 2002;**40**(6):1056–60.
3. Scarano F. *Overview of PIV in supersonic flows*. Berlin Heidelberg: Springer; 2007. p. 445–63.
4. Schrijer FFJ, Scarano F, Van Oudheusden BW, Bannink WJ. Application of PIV in a hypersonic double-ramp flow. Reston: AIAA; 2005 Report No.: AIAA-2005-3331.
5. Schrijer FFJ, Scarano F, Van Oudheusden BW. Application of PIV in a Mach 7 double-ramp flow. *Exp Fluids* 2006;**41**(2):353–63.
6. Schrijer FFJ, Walpot LMGFM. Experimental investigation of the supersonic wake of a reentry capsule. Reston: AIAA; 2010 Report No.: AIAA-2010-1251.
7. Wang D, Xia Z, Zhao Y, Wang B, Zhao Y. Imaging of the space-time structure of a vortex generator in supersonic flow. *Chin J Aeronaut* 2012;**25**(1):57–63.
8. Urban WD, Mungal MG. Planar velocity measurements in compressible mixing layers. *J Fluid Mech* 2001;**431**(486):189–222.
9. Scarano F, Van Oudheusden BW. Planar velocity measurements of a two-dimensional compressible wake. *Exp Fluids* 2003;**34**(3):430–41.
10. Ghaemi S, Schmidt-Ott A, Scarano F. Nanostructured tracers for laser-based diagnostics in high-speed flows. *Meas Sci Technol* 2010;**21**(10):105403.
11. Ragni D, Schrijer F, Van Oudheusden BW, Scarano F. Particle tracer response across shocks measured by PIV. *Exp Fluids* 2011;**50**(1):53–64.
12. Melling A. Tracer particles and seeding for particle image velocimetry. *Meas Sci Technol* 1997;**8**(12):1406–16.
13. Dring RP. Sizing criteria for laser anemometry particles. *J Fluid Eng* 1982;**104**(1):15–7.
14. Tedeschi G, Gouin H, Elena M. Motion of tracer particles in supersonic flows. *Exp Fluids* 1999;**26**(4):288–96.
15. Amatucci VA, Dutton JC, Kuntz DW, Addy AL. Two-stream, supersonic, wake flow field behind a thick base. I-General features. *AIAA J* 1992;**30**(8):2039–46.
16. Chen F, Liu H, Rong Z. Development and application of nanoparticle tracers for PIV in supersonic and hypersonic flows. Reston: AIAA; 2012 Report No.: AIAA-2012-0036.
17. Wooldridge J. *Introductory econometrics: A modern approach*. Mason (OH): Cengage Learning; 2012.
18. Stokes GG. On the effect of the internal friction of fluids on the motion of pendulums. *Trans Cambridge Philos Soc* 1851;**9**(2):8.
19. Koike S, Takahashi H, Tanaka K, Hirota M, Takita K, Masuya G. Correction method for particle velocimetry data based on the Stokes drag law. *AIAA J* 2007;**45**(11):2770–7.
20. Humble RA, Scarano F, Van Oudheusden BW. Particle image velocimetry measurements of a shock wave/turbulent boundary layer interaction. *Exp Fluids* 2007;**43**(2–3):173–83.
21. Mathijssen T, Bannink WJ, Scarano F. Investigation of a sharp-edged delta wing in a supersonic flow using stereo PIV. Reston: AIAA; 2009 Report No.: AIAA-2009-3896.
22. Loth E. Compressibility and rarefaction effects on drag of a spherical particle. *AIAA J* 2008;**46**(9):2219–28.